A&A, 693, A304 (2025)
https://doi.org/10.1051/0004-6361/202449818

Astronomy & Astrophysics

Sequential dissociation of ionized benzonitrile: New pathways to reactive interstellar ions and neutrals

D. Bou Debes[1], M. Mendes[2], R. Rodrigues[2], J. Ameixa[2,3], L. M. Cornetta[4], F. Ferreira da Silva[2], and S. Eden[1,⋆]

[1] School of Physical Sciences, The Open University, Walton Hall, Milton Keynes, MK7 6AA, UK
[2] CEFITEC, Departamento de Física, NOVA School of Science and Technology, Universidade NOVA de Lisboa, 2829-516 Caparica, Portugal
[3] Institute of Chemistry, Hybrid Nanostructures, University of Potsdam, Karl-Liebknecht-Str. 24-25, 14476, Potsdam, Germany
[4] Instituto de Física, Universidade de São Paulo, Rua do Matão 1731, 05508-090, São Paulo, Brazil

Received 29 February 2024 / Accepted 6 December 2024

ABSTRACT

Since benzonitrile's discovery in the interstellar medium (ISM) in 2018, several studies have explored the strongest unimolecular dissociations of its radical cation ($C_6H_5CN^{\bullet+}$). However, sequential dissociation processes, which become important when ionization occurs with significant excess energy transfer, have received almost no attention to date. The present metastable dissociative ionization experiments reveal 14 different dissociations, of which 11 have never been observed before. Nine of these new reactions involve the dissociation of a fragment ion. A notable result shows that $C_4H_2^{\bullet+}$ production (the second most intense fragment ion in conventional mass spectra without metastable dissociation analysis) derives from sequential dissociation via $C_6H_4^{\bullet+}$, as well as from the previously reported unimolecular dissociation of $C_6H_5CN^{\bullet+}$. Furthermore, our experiments demonstrate new pathways that produce astrochemically important neutrals including HCN/CNH and $CN^{\bullet}$, as well as revealing $CH^{\bullet}$ and $C_3H^{\bullet}$ production from ionized benzonitrile for the first time. In addition to the metastable dissociation experiments, we applied density functional theory to calculate two sequential dissociation routes and report the results of our detailed analysis of the peak shapes in a conventional mass spectrum of benzonitrile. The latter enabled the dominant ion to be identified in peaks with nearest-integer m/z values that match two conceivable ions. The present identification of $C_6H_2N^+$ production using this approach allows its presence in the ISM to be inferred for the first time. This paper extends our understanding of how the dissociative ionization of benzonitrile can contribute to the abundances of radicals and other reactive species in interstellar environments.

Key words. astrochemistry – molecular processes – methods: laboratory: molecular – ISM: molecules – ultraviolet: ISM

1. Introduction

Benzonitrile's detection in the Taurus molecular cloud by McGuire et al. (2018) represented the first observation of a nitrogen-containing aromatic molecule in the interstellar medium (ISM). It has since been identified in several other molecular clouds (Burkhardt et al. 2021) and has been proposed as a possible precursor species for reactions that produce interstellar nitrogen-containing polycyclic aromatic hydrocarbons (McGuire et al. 2018; Jacovella et al. 2022). Rap et al. (2024) have demonstrated that reactions of o-benzyne$^{\bullet+}$, an intense fragment from ionized benzonitrile, with the widely observed interstellar molecule acetylene can produce polycyclic aromatic hydrocarbons. Characterizing radiation-induced processes in benzonitrile can therefore have applications for modeling the production of reactive species in diverse astronomical environments, as well as the possible formation pathways of more complex stable molecules.

The current astrochemical interest in benzonitrile's radiation response has inspired recent gas-phase studies of the molecule's UV absorption and photoelectron spectroscopies (Rajasekhar et al. 2022; Kamer et al. 2023), as well as investigations of the fragmentation pathways of excited protonated benzonitrile (Jacovella et al. 2022) and the electronic and vibrational spectra of benzonitrile$^{\bullet+}$ (Daly et al. 2024). Furthermore, two papers in 2023 combined experiment and theory to explore the dissociative ionization channels of benzonitrile (C_6H_5CN, 103 amu, shown schematically in Fig. 1a). First, Rap et al. (2023) used IR spectroscopy to identify the structures of the ions with m/z 102 and 77-75 that are produced by electron ionization (EI) at 15 or 50 eV. They complemented their experiments with calculated reaction pathways (B3LYP-GD3/N07D with zero-point correction) that lead to unimolecular loss of $H^{\bullet}$, $CN^{\bullet}$, CNH, HCN, and C_2H_4 from benzonitrile$^{\bullet+}$. In addition, they ran molecular dynamics simulations of excited benzonitrile$^{\bullet+}$ (internal energy between 8 and 9 eV; time 500 ps to 1 ns) that indicated ten different unimolecular dissociations, including C_2H_2 loss and C_3NH loss. Kamer et al. (2023) measured threshold photoelectron-photoion coincidence mass spectra in the photon energy range 13.75–19.75 eV. They applied a Rice–Ramsperger–Kassel–Marcus statistical model to their data to determine the lowest energy barriers associated with seven fragment ions (m/z 77-75, 52-50, and 39). They then assigned specific fragment ion structures by comparing the experimental barriers with calculated reaction pathways (B3LYP/6-311++G(d,p) refined by CBS-QB3 with zero-point correction) for unimolecular dissociations of benzonitrile$^{\bullet+}$. These recent papers added substantially to the prior EI (Schug 1964; Baldwin 1979; Inoue et al. 1983; Martin & O'Malley 1984),

⋆ Corresponding author; sam.eden@open.ac.uk

photoionization (Rosenstock et al. 1980), and multi-photon ionization (MPI; Martin & O'Malley 1984) studies of benzonitrile's dissociative ionization, most of which focused primarily on direct HCN loss. However, whereas the strongest unimolecular dissociations of benzonitrile$^{\bullet+}$ have been analyzed in some detail, the present work is the first to explore its sequential fragmentation.

The most significant experiments in our study employed a reflectron time-of-flight (TOF) mass spectrometer to identify dissociations that took place several microseconds after ionization. This approach simultaneously reveals the m/z value of the dissociation's precursor ion (the metastable ion) and its product ion. Hence, it reveals dissociations that belong to sequential fragmentation pathways and demonstrates unimolecular dissociations of the excited parent ion. This extra information compared with conventional mass spectrometry comes at a cost, however. The resolving power of a given reflectron TOF instrument is much lower for the precursor and product ions of metastable dissociations than it is for ions that do not dissociate between leaving the mass spectrometer's ion source and reaching the detector. Therefore, to maximize resolution, we chose to multi-photon-ionize benzonitrile in focused laser pulses. This method yields the best resolution achievable with our apparatus because (i) ionization occurs in a small and precisely defined volume and (ii) the ion cloud produced by a laser pulse crossing the target gas is not allowed to expand before extraction from the ion source.

In addition to the metastable dissociation experiments, the high resolution of the present MPI-TOF system enabled us to demonstrate the atomic composition of various fragment ions from benzonitrile for the first time. The present work also includes a comparison between conventional EI and MPI mass spectra. The comparison did not yield any evidence suggesting that a dissociation visible in our MPI data depends uniquely on that energy deposition process, and hence it supports the generality of our conclusions about the fragmentation of excited benzonitrile$^{\bullet+}$. Finally, we performed density functional theory (DFT) calculations to describe the reaction pathways of two notable sequential dissociation routes that were visible in our experiments.

2. Experimental methods

The measurements were carried out using crossed beam experiments at the Open University (OU) and at Universidade NOVA de Lisboa. They have been presented in previous publications (Bockova et al. 2019; Pereira-da Silva et al. 2021) and are only described briefly here.

The OU apparatus featured one change compared with previous publications by the group: the molecular target was produced at room temperature using a simple effusive nozzle. The nozzle was mounted in the grounded backplate of the mass spectrometer (originally built by Kore Technology Ltd.), as indicated in Fig. 1b. Benzonitrile molecules in the ion source region between the backplate and the extraction grid were multi-photon ionized in focused 225 nm pulses (average fluence 10^7 W cm^{-2}) from a Nd-YAG-pumped dye laser with a frequency doubling unit (Continuum Powerlite II 8000 - Sirah Cobra-Stretch). The ion signals were timed using a Fast Comtec P7887 time-to-digital conversion card. The data acquisition system was based on a LabView application interfacing with the time-to-digital conversion card and a laser pulse energy meter (Spectrum Detector SPJ-D-8). Background ion signals due to residual gas in the chamber were negligible.

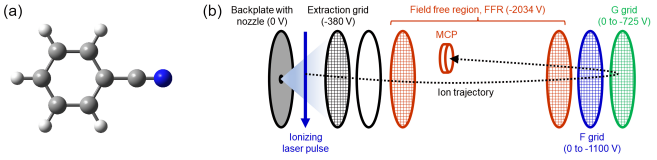

Fig. 1. Molecular structure (a) of benzonitrile (C_6H_5CN) and sketch of the TOF experiment (b) that was used to identify microsecond-timescale (metastable) dissociations following the MPI of benzonitrile from an effusive nozzle.

The reflection voltage in the OU mass spectrometer (which can be applied to either the F grid or the G grid; see Fig. 1b) can be adjusted to investigate metastable fragmentation. This approach exploits the fact that an ion produced by a dissociation in the field-free region (FFR; 0.9−13.8 µs after the laser pulse in the present experiments) reaches the end of the FFR with lower kinetic energy than an equivalent ion produced by a dissociation in the ion source region, and hence can be reflected in a weaker field. A simulation was developed in Python 3 (Van Rossum & Drake 2009) to identify metastable dissociations visible in experimental maps of ion counts against flight time and reflection voltage. The initial inputs are the distances within the mass spectrometer, the electrode voltages (except for the reflection voltage), and the crossing position of the laser beam with the effusive beam of benzonitrile molecules. The crossing position was determined by measuring the reflection voltage at which the intact parent ion signal (benzonitrile$^{\bullet+}$) was extinguished, following the method described by Ryszka et al. (2016). The next step is to input one or more candidate dissociations (specific combinations of precursor and product ion m/z values) that might take place in the FFR. The program then generates a map of flight-time against reflection voltage that can be overlaid onto the experimental map. Different candidate dissociations are tested iteratively until the best possible match is achieved between the simulated and experimental maps (e.g., Fig. 4).

Photon absorption at 225 nm (5.51 eV) coincides with the low-energy extreme of the π–$\pi*$ band in Rajasekhar et al. (2022)'s UV absorption spectrum, accessing benzonitrile's second-lowest-lying singlet excited state (S_2). While the dynamics of this state have not been fully elucidated to date, internal conversion to S_1 (4.54 eV above S_0; Rajasekhar et al. 2022) is plausible prior to subsequent photon absorption at the present laser fluence. A previous study of phenylacetylene (identical to benzonitrile except benzonitrile's N is replaced with CH) suggests that the S_1 state of benzonitrile will have a much longer lifetime than the present laser pulse width (Hofstein et al. 2008). Therefore, we expect that MPI of benzonitrile involves ionization from either S_2 or S_1 in the present experiments. Both of these states have similar calculated geometries to the neutral electronic ground state in terms of the C-N bond length, the C-CN bond length, and the C-C-N bond angle (Rajasekhar et al. 2022). Previous experiments using the OU apparatus to probe uracil, a similarly sized aromatic molecule with a similar ionization energy (9.15 eV in Jochims et al. 2005 compared with (9.72 ± 0.02) eV for benzonitrile in Kamer et al. 2023), indicated that two- and three-photon absorption (11.0 and 16.5 eV at 225 nm) dominated ion production (Barc et al. 2013) but higher-order photon absorption was not negligible.

The NOVA experiment was used here for 70 eV EI measurements of benzonitrile in an effusive beam. The setup consists of a thermionic electron source and a home-built trochoidal electron monochromator, coupled with an Orthogonal Reflectron TOF

Mass Spectrometer (OReToFMS) manufactured by KORE Technology Ltd. The experiment was heated to 368 K to prevent possible benzonitrile condensation on the electron monochromator electrodes.

The benzonitrile samples in both experiments were purchased from Sigma-Aldrich with a stated purity ≥99%. The vapor above a liquid sample at room temperature was introduced into the interaction region via an effusive nozzle connected to a leak valve after at least three freeze-pump-thaw cycles. The base pressure in the experiments was in the range $1–9 \times 10^{-8}$ mbar, and the pressure during the benzonitrile measurements was in the range $9 \times 10^{-8}–7 \times 10^{-7}$ mbar.

3. Theoretical methods

To explore the reaction pathways of some of the dissociation channels observed in the present experiments, DFT calculations were conducted using Gaussian software (Frisch et al. 2016). Reactants, products, and transition states (TSs) were optimized at the B3LYP level of theory (Becke 1993) with the 6-311++G(2df,2p) basis set. The large basis set was chosen to ensure convergence to energy limits and is supported by good agreements with experimental ionization energies (Díaz-Tinoco et al. 2016). Frequency calculations were performed on all the obtained structures to confirm that the reactants and products correspond to minima on the potential energy surface and that each TS is a saddle point on the potential energy surface. Furthermore, each TS was verified by examining the vibrational mode associated with the imaginary frequency and subsequently performing an intrinsic reaction coordinate calculation (Fukui 1981) to ensure that the reaction path descends from the TS to the correct reactant and product. The computed energies displayed in the reaction pathways have been zero-point-corrected to aid comparisons with recent calculations of unimolecular dissociations of benzonitrile$^{\bullet+}$ (Rap et al. 2023; Kamer et al. 2023).

4. Results and discussion

4.1. Electron ionization (EI) and multi-photon ionization (MPI) mass spectra

Figure 2 shows EI (panel a) and MPI (panel b) mass spectra of benzonitrile. The reflection voltage in the MPI measurement was set to allow the detection of prompt ions (defined here as any ions that do not dissociate later than 100 ns after MPI). In both of the mass spectra, the ratio of the m/z 104 signal over the m/z 103 signal matches the expected population of benzonitrile isotopes (8%). This supports the absence of saturation effects and of protonated benzonitrile (a prominent fragment from benzonitrile cluster ions (Bou-Debes et al., in prep.). Indeed, no peaks that could suggest the presence of clusters were observed in the mass spectra.

Figure 2 shows that the most intense peaks (notably at m/z 103, 76 and 50) and the main ion groups produced by EI and MPI are consistent with each other. The differences in relative peak intensities can be linked to the ion acceptance functions of the two mass spectrometers and/or to the energy deposition in the two ionization processes. Seven EI peaks were not visible in the MPI measurements (e.g., at m/z 84 and 85 in Fig. 2), and we attributed them to high energy deposition processes such as double ionization, which occur preferentially in 70 eV electron collisions compared with the MPI conditions studied here. These seven EI peaks are discussed in Appendix A. Considering the signal-to-noise ratios in the MPI data and the EI data, we did not see evidence for any fragment ion channels that are accessed by MPI only. This suggests that the conclusions from our MPI experiments (ion identifications based on Gaussian peak fitting in this section as well as specific fragmentations revealed by the metastable dissociation results in Sect. 4.2) also apply to EI. Moreover, the general similarity of the MPI and EI mass spectra in Fig. 2 is consistent with our expectation that MPI in the present laser pulse conditions involves ionization from neutral electronic excited states that have similar geometries to benzonitrile's neutral ground state (discussed briefly in Sect. 2).

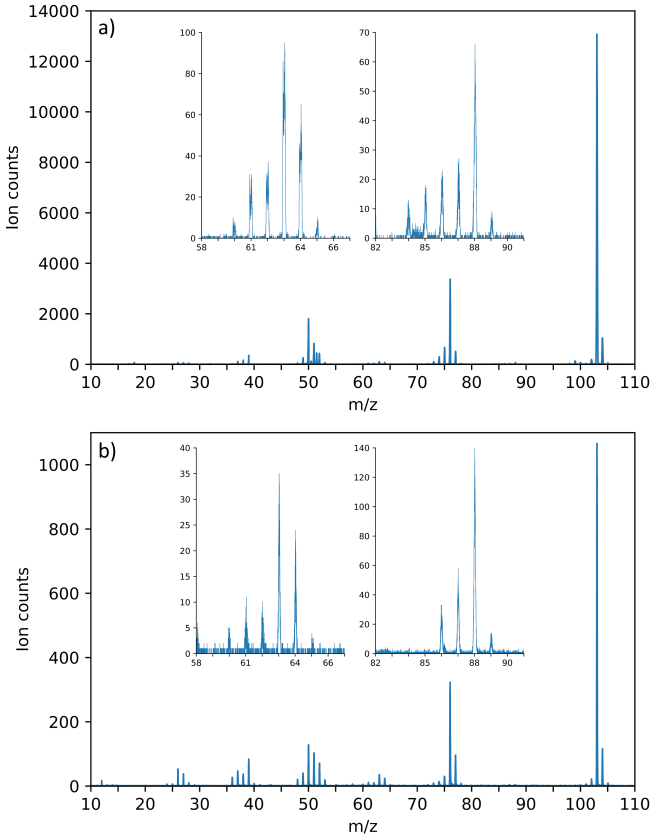

Fig. 2. EI (a) and MPI (b) mass spectra of benzonitrile. To show the m/z 82–91 range with better statistics, the relevant insert in panel b comes from a separate MPI measurement with a higher benzonitrile target pressure.

Many of the peaks in the benzonitrile mass spectra have m/z values that, when obtained to the nearest integer, could be assigned to ions with different combinations of atoms. The mass resolution of the present MPI experiments (e.g., full width half maximum $\Delta m/z$ = 0.089 for the benzonitrile$^{\bullet+}$ peak) was not sufficient to completely separate peaks according to their atomic compositions. However, by applying Gaussian fits to MPI peaks that had good signal-to-noise ratios in the context of the narrow bin width and that showed no signs of asymmetry (e.g., tail features), we were able to obtain precise m/z values for the peaks' centers. This enabled us to identify the atomic composition of the ion that was mainly responsible for the peak. For example, Fig. 3 shows Gaussian fits of three peaks that are highlighted in the discussion below. The uncertainty of ±m/z 0.005 on the center m/z values of the fitted peaks is mainly linked to the calibration function relating TOF to $(m/z)^{\frac{1}{2}}$. The calibration relied on obtaining center m/z values for peaks with unique possible atomic compositions such as benzonitrile$^{\bullet+}$ (m/z 103.042) and CH^+ (m/z 13.008). Tables C.1 and C.2 list all the prompt ion peaks in our

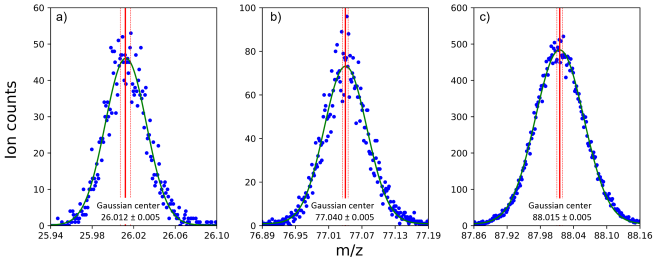

Fig. 3. Details of the MPI peaks from benzonitrile with nearest-integer m/z values of 26, 77, and 88. The experimental data points are shown in blue and the Gaussian fits in green. (a) The fitted center (m/z 26.012 ± 0.005) indicates that $C_2H_2^{\bullet+}$ (26.016) dominates over any $CN^{\bullet\bullet+}$ (26.003). (b) The fitted center (m/z 77.040 ± 0.005) indicates that $C_6H_5^+$ (77.039) dominates over any $C_5H_3N^{\bullet+}$ (77.027). (c) The fitted center (m/z 88.015 ± 0.005) indicates that $C_6H_2N^+$ (88.019) dominates over any $C_7H_4^{\bullet+}$ (88.031).

MPI mass spectra and, where possible, provide center m/z values to aid assignments. The tables also note any relevant ions that have been observed in the ISM to date (to our knowledge).

The seven fragment ion assignments by Martin & O'Malley (1984) that are quoted in Tables C.1 and C.2 were mainly based on the authors recognizing analogous peak patterns in nonresonant MPI mass spectra of benzonitrile, benzene, phenylacetylene, toluene, t-butyl benzene, and diphenylmethane. Four of their deductions ($C_6H_4^{\bullet+}$, $C_4H_4^{\bullet+}$, $C_4H_3^+$, and $C_4H_2^{\bullet+}$) have already been supported by subsequent experiments, most recently by Kamer et al. (2023). The present Gaussian peak fitting enables us to demonstrate that Martin & O'Malley (1984)'s remaining deductions ($C_4H_2N^+$, $C_3H_3^+$, and $C_2H_2^{\bullet+}$ as shown in Fig. 3a) are also correct. Additionally, the present measurements confirm the $C_6H_5^+$ assignment (Kamer et al. 2023; Rap et al. 2023; Molenaar-Langeveld et al. 1986) (Fig. 3b), and this dissociation channel is discussed further in Sect. 4.2. In addition to the assignments mentioned above, the Gaussian peak fitting allowed us to identify the dominant ions responsible for nine peaks that are visible in previous mass spectra but (i) have never been assigned before and (ii) could be attributed to different atomic combinations based on their nearest-integer m/z values. $C_4H_3N^{\bullet+}$, $C_4H_5^+$, $C_3H_4^{\bullet+}$, $C_3H_2^{\bullet+}$ and $C_2H_3^+$ have one fewer or one extra hydrogen atom compared with previously assigned ions, so these assignments are not surprising. None of the neighboring peaks of $CH_2^{\bullet+}$, CH_3^+, $C_6HN^{\bullet+}$, and $C_6H_2N^+$ have been assigned before. $C_6H_2N^+$ is of particular interest because in Sect. 4.2 and Table C.3 we demonstrate that nearest-integer m/z 88 ions are interim species in sequential dissociative ionization pathways that yield neutral HCN and/or CNH products.

Further to its role in sequential dissociation pathways, the present identification of $C_6H_2N^+$ (Fig. 3c) from benzonitrile is interesting with respect to the diversity of species in the ISM. Any dissociative ionization product of a known interstellar molecule must also be present in the ISM, even if its low abundance and/or the lack of spectroscopic reference data currently prevent its direct observation. Whereas $C_6HN^{\bullet+}$ is visible in Couturier-Tamburelli et al. (2014)'s 70 eV EI mass spectrum of HC_7N, the only reported interstellar molecules aside from benzonitrile that could fragment to form $C_6H_2N^+$ are $C_{10}H_7CN$ (1-cyanonaphthalene and 2-cyanonaphthalene) and $C_{11}H_{12}N_2O_2$ (tryptophan, based on a tentative spectral attribution) (McGuire et al. 2021; Iglesias-Groth 2023). The mass spectra of these three molecules contain weak peaks at nearest-integer m/z 88 (Wallace 2024; Tamuliene et al. 2015) but, to our knowledge, no work has been carried out to distinguish possible $C_6H_2N^+$ from alternative ions such as $C_7H_4^{\bullet+}$, $C_5N_2^{\bullet+}$, or $C_6O^{\bullet+}$. Hence, the present analysis of benzonitrile's MPI mass spectrum provides the first evidence supporting the presence of $C_6H_2N^+$ in the ISM.

In addition to considering the fragment ions produced from benzonitrile, it is useful to note two ions that are absent from Table C.2. Our experiments show that the dissociative ionization of benzonitrile is not a significant source of two nitrogen-containing ions that have been observed in the ISM: $CN^{\bullet\bullet+}$ (m/z 26.003; our Fig. 3a; Dopita & Sutherland 2013) and $C_3H_2N^+$ (m/z 52.019; Kawaguchi et al. 1993). A general trend is apparent from the table: small fragment ions from benzonitrile tend not to contain N. From the 23 peaks observed with m/z ≤61, we can identify 22 different ions conclusively and none of these contain N. Although some exceptions might have been anticipated, this trend is not surprising in view of nitrogen's electronegativity compared with carbon and hydrogen. It should also be noted that it is generally energetically favorable for the charge to reside on the larger fragment following the dissociation of an ion (larger molecules generally have lower ionization energies), and this effect is likely to dominate charge localization for fragments with masses greater than 61 amu.

4.2. Metastable dissociation experiments

To our knowledge, the only metastable dissociation channel of ionized benzonitrile that has been reported in the literature is m/z 103 → 76 (Schug 1964; Baldwin 1979) attributed to competing HCN/CNH loss from benzonitrile$^{\bullet+}$ (Rap et al. 2023). The curved bands in Fig. 4 reveal many more metastable dissociations following MPI of benzonitrile. The two maps in the figure correspond to different focusing conditions in the reflectron part of the mass spectrometer. In the Fig. 4b measurements, ions were allowed to penetrate farther into the reflectron before changing direction and traveling toward the detector. This arrangement yielded higher signals for metastable dissociation products with high m/z values, and lower signals for those with low m/z values. Any given metastable dissociation channel produces a band at longer flight times in Fig. 4b than in Fig. 4a.

Table C.3 lists the 17 different metastable dissociations observed in our MPI experiments, including three dissociations of isotopes. Four of these dissociations are visible in both of the panels in Fig. 4 (e.g., bands *E* and *M* correspond to the same dissociation). Comparing the experimental data with the simulated flight times provides the nearest-integer m/z values of the precursor ions and of the product ions. To help assign specific atomic compositions in the table, we assumed that the ions involved in the observed metastable dissociations are the same as the ions with the same nearest-integer m/z values that have been identified in prompt dissociative ionization experiments (present results and earlier work summarized in Tables C.1 and C.2).

As well as listing m/z values of the precursor and the product ions for each of the observed metastable dissociations, Table C.3 provides the mass of the neutral product. This assignment applies the standard assumption that the metastable dissociation of an ion involves the loss of a single neutral (Lindon et al. 2000). Metastable dissociation only occurs when the internal energy of the precursor ion is very close to the barrier for a given dissociation, and this generally means that insufficient energy is available for a subsequent dissociation of the product ion or of its neutral counterpart.

The cyano radical ($CN^{\bullet}$) is believed to play an important role in diverse chemical reactions in the ISM, so its production

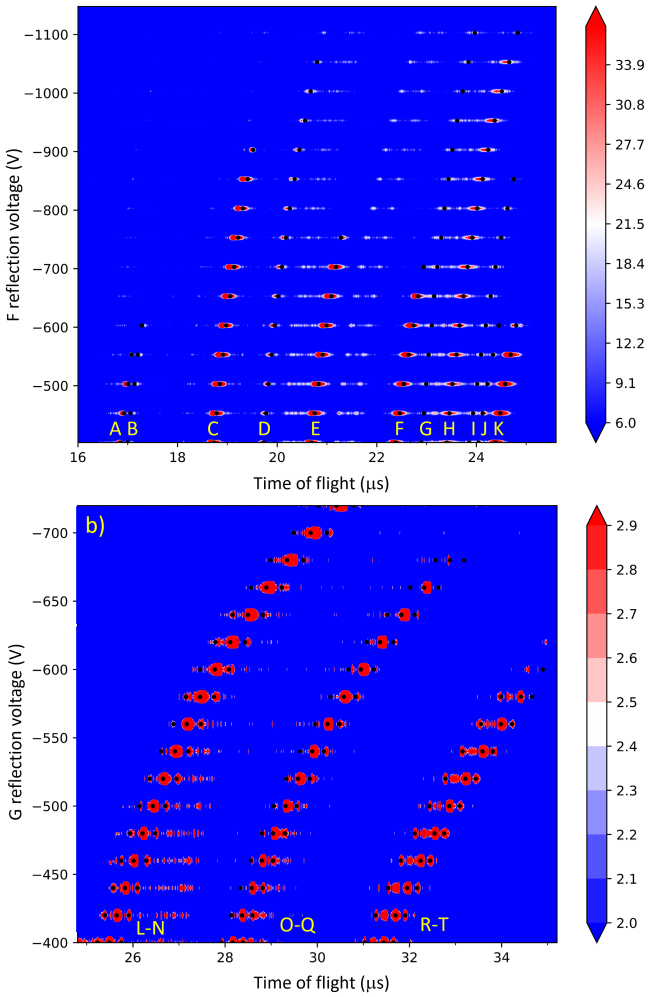

Fig. 4. MPI signals from benzonitrile mapped against flight-time and reflection voltage. The signals (ion counts per 16 ns time bin) are indicated by red and white features, and the curved bands correspond to metastable dissociations in the FFR of the mass spectrometer. The simulated flight times for the metastable dissociations that agree best with the experimental bands are indicated by black dots and listed in Table C.3. Map (a) was recorded with the reflection voltage applied to Grid F in the mass spectrometer (see Fig. 1b), whereas map (b) was recorded with the reflection voltage applied to Grid G.

mechanisms are of special interest. For example, due to its reactivity with molecules possessing double or triple bonds between carbon atoms, $CN^{\bullet}$ is understood to be involved in the formation of cyanopolyynes. These molecules are present in high-mass star-forming regions and hot cores and have been proposed as chemical clocks to determine the ages of those objects (Paron et al. 2021). 70 eV electron-impact luminescence has been used previously to identify $CN^{\bullet}$ from benzonitrile (Inoue et al. 1983), but those experiments did not distinguish its production mechanism. Band *T* in Fig. 4 and Table C.3 contains a combination of m/z 104 → 77 and 103 → 77 dissociations. Combining this observation with the fact that $C_6H_5^+$ production dominates over any possible $C_5H_3N^{\bullet+}$ contribution (Fig. 3c) enables us to identify the $C_6H_5CN^{\bullet+} \rightarrow C_6H_5^+ + CN^{\bullet}$ dissociation channel (as opposed to any conceivable sequential loss of C and N from benzonitrile$^{\bullet+}$). Our result supports Kamer et al. (2023)'s assignment based on comparing the experimental photoionization threshold for m/z 77 ion production with the DFT-calculated barrier for unimolecular $CN^{\bullet}$ loss from benzonitrile$^{\bullet+}$.

The present experiments provide evidence for a second mechanism for $CN^{\bullet}$ production by dissociative ionization of benzonitrile. Band *L* is due to m/z 75 → 49 dissociation, Rap et al. (2023)'s IR spectroscopy of benzonitrile's ionization products revealed a linear $HC_5N^{\bullet+}$ structure; there is no evidence here or in the literature suggesting $C_6H_3^+$ production from benzonitrile, and the m/z 49 product can only be C_4H^+. Therefore, the band can be assigned to $C_5HN^{\bullet+} \rightarrow C_4H^+ + CN^{\bullet}$ with confidence. In addition to this new $CN^{\bullet}$ production mechanism, we see the loss of a 26 amu neutral ($CN^{\bullet}$ or C_2H_2) from $C_7H_2N^+$ (bands *J* and *R*). Further experiments or calculations are required to determine if this is an additional source of $CN^{\bullet}$ from ionized benzonitrile.

Fragmentation to form $C_6H_4^{\bullet+}$ (m/z 76) and HCN/CNH has received more attention in the literature than any other dissociative ionization channel of benzonitrile. As with $CN^{\bullet}$ (Ziurys 2006), both HCN (Ziurys 2006) and CNH (Schilke et al. 2001) have been observed in the ISM and can participate in diverse reactions, so there is significant interest in their interstellar production mechanisms. As well as confirming the well-known unimolecular dissociation (bands *K* and *S*), we report HCN/CNH production via a sequential dissociation pathway of benzonitrile$^{\bullet+}$ for the first time. The precursor ion in the m/z 88 → 61 dissociation (bands *F* and *P*) can be assigned to $C_6H_2N^+$ on the basis of the Gaussian fitting described in Sect. 4.1 and the product ion can only be C_5H^+, so the neutral counterpart can be identified as HCN or CNH. These reactions are explored using DFT in Sect. 4.3 (Fig. 6).

In addition to the new pathway described above, our results reveal two further dissociations that might produce HCN/CNH. Comparing the relatively weak experimental band *O* with the simulated flight times indicated two possible assignments for the precursor ion: m/z 87 or 86. Hence, the neutral product could be HCN, CNH, $CN^{\bullet}$, or C_2H_2. The m/z 64 → 37 dissociation (band *C*) yields a 27 amu neutral, but we have no evidence to assign it to HCN/CNH as opposed to $C_2H_3^{\bullet}$. These possible dissociations would be interesting subjects for future experiments or calculations.

Kamer et al. (2023)'s comparisons of photoionization thresholds with calculated dissociation energies indicated seven unimolecular dissociations of benzonitrile$^{\bullet+}$. The present experiments confirm three of these channels: $C_6H_5CN^{\bullet+} \rightarrow C_6H_5^+ + CN^{\bullet}$, $C_6H_5CN^{\bullet+} \rightarrow C_6H_4^{\bullet+}$ + HCN/CNH, and $C_6H_5CN^{\bullet+} \rightarrow C_4H_2^{\bullet+} + C_3H_3N$. The lack of evidence in the present results for Kamer et al. (2023)'s reported unimolecular dissociations producing $HC_5N^{\bullet+}$ + (m/z 75), $C_4H_4^{\bullet+}$ (m/z 52), $C_4H_3^+$ (m/z 51), and $C_3H_3^+$ (m/z 39) is most likely linked to the fact that a given dissociation only occurs on a microsecond timescale if the precursor ion's internal energy is very close to the relevant dissociation barrier. Hence, we speculate that the present MPI scheme produces negligible populations of benzonitrile$^{\bullet+}$ with internal energies close to the barriers for these four unimolecular dissociations.

Table C.3 reveals two unimolecular dissociations of benzonitrile$^{\bullet+}$ for the first time: m/z 103 → 62 ($C_5H_2^{\bullet+}$ or C_4N^+) and m/z 103 → 37 or 38 (C_3H^+, $C_3H_2^{\bullet+}$, $C_2N^{\bullet+}$). In the latter dissociation (band *G*), it seems initially surprising that the positive charge has remained on the smaller fragment but Kamer et al. (2023)'s attribution of $C_3H_3^+$ to unimolecular dissociation of the parent ion provides a precedent for this. The most intriguing aspects of the m/z 103 → 37 or 38 dissociation are the possible neutral byproducts: $C_4H_4N^{\bullet}$, C_4H_3N, or $C_5H_5^{\bullet}$. Hendrix et al. (2020)'s recent theoretical study of the isomers of $C_4H_4N^{\bullet}$, $C_4H_4N^-$, and $C_4H_4N^+$ was motivated by their possible presence in dark molecular clouds and in the atmospheres of

planetary bodies (noting the m/z 66 signal in mass spectrometry measurements of Titan's atmosphere from the Cassini–Huygens mission). However, none of these reactive species have been observed conclusively in extraterrestrial atmospheres or in the ISM. Similarly, no observations of interstellar C_4H_3N or $C_5H_5^{\bullet}$ have been reported to date. Future investigations into which of these neutrals are produced through the dissociative ionization of benzonitrile would be valuable.

Combining our results with Kamer et al. (2023)'s brings the number of experimentally verified unimolecular dissociations of benzonitrile$^{\bullet+}$ to nine. No dissociations of fragment ions of benzonitrile have been identified previously, and Table C.3 reveals nine such dissociations (not including dissociations of isotopes). Therefore, sequential fragmentation processes play a major role in determining the diversity of ions and neutrals that stem from the dissociative ionization of benzonitrile. Furthermore, it is interesting that we see a sequential dissociation step (bands *E* and *M*: $C_6H_4^{\bullet+} \rightarrow C_4H_2^{\bullet+} + C_2H_2$) that competes with unimolecular dissociation of benzonitrile (band *H*) to produce $C_4H_2^{\bullet+}$ (m/z 50, the third most intense peak in typical prompt mass spectra of benzonitrile such as Fig. 2).

In addition to its role in producing one of benzonitrile's main fragment ions, the present observation of $C_6H_4^{\bullet+} \rightarrow C_4H_2^{\bullet+} + C_2H_2$ is the first experimental demonstration of neutral C_2H_2 production from ionized benzonitrile. Similarly, band *D* ($C_6H^+ \rightarrow C_3^{\bullet+} + C_3H^{\bullet}$) provides the first evidence for neutral $C_3H^{\bullet}$ production from benzonitrile. Therefore, sequential dissociative ionization of benzonitrile must contribute to the interstellar budget of acetylene (the only stable form of C_2H_2), as well as propynylidyne and/or cyclopropynylidyne, all of which have been observed in the ISM (Ridgway et al. 1976; Ziurys 2006; Mangum & Wootten 1990).

4.3. Calculated sequential fragmentation pathways

We carried out DFT calculations to identify reaction pathways that can lead to several interesting dissociations reported in Sect. 4.2. Our first step was to consider the dissociation of benzonitrile$^{\bullet+}$ into $C_6H_4^{\bullet+}$ (specifically the o-benzyne$^{\bullet+}$ isomer) and HCN or CNH. Reassuringly, we obtained the same reaction pathways that have been calculated recently by both Rap et al. (2023) and Kamer et al. (2023) using alternative levels of theory and basis sets (see Sects. 1 and 3). Our calculated dissociation energies with respect to ground-state benzonitrile$^{\bullet+}$ lie between the previously calculated energies (e.g., 3.77 eV for o-benzyne$^{\bullet+}$ production with HCN, compared with 3.71 eV, Kamer et al. 2023; and 4.0 eV, Rap et al. 2023).

Three notable dissociations in Table C.3 can occur in a sequence: benzonitrile$^{\bullet+} \rightarrow$ (HCN/CNH +) $C_6H_4^{\bullet+} \rightarrow$ (C_2H_2 +) $C_4H_2^{\bullet+} \rightarrow$ ($CH^{\bullet}$ +) C_3H^+. This sequence includes the two strongest fragment ions in conventional mass spectra of benzonitrile: $C_6H_4^{\bullet+}$ and $C_4H_2^{\bullet+}$ (Fig. 2). Rap et al. (2023) identified two isomers of $C_6H_4^{\bullet+}$ from benzonitrile$^{\bullet+}$: o-benzyne$^{\bullet+}$ (maintaining the parent ion's 6-carbon ring) and bicyclic m-benzyne$^{\bullet+}$ (featuring a 5-carbon ring), but the peaks associated with o-benzyne$^{\bullet+}$ were strongest in their IR spectrum. Therefore, we chose to focus our DFT calculations on the loss of C_2H_2 from o-benzyne$^{\bullet+}$ to form $C_4H_2^{\bullet+}$, and then the subsequent loss of $CH^{\bullet}$ (Fig. 5).

No previous publications have explored the reactions of $C_6H_4^{\bullet+}$ fragments from benzonitrile$^{\bullet+}$, but one dissociation of $C_6H_4^{\bullet+}$ from a different source has been reported. Liu et al. (2002) observed $C_6H_4^{\bullet+}$ production through photolysis of Mg^+-difluorobenzene complexes. They also detected $C_4H_2^{\bullet+}$ products

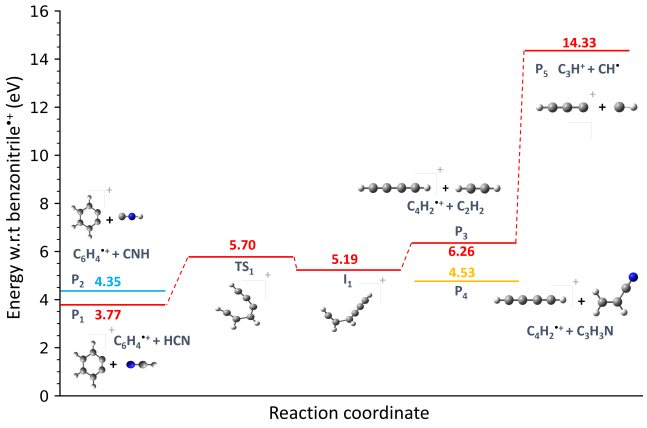

Fig. 5. Calculated reaction pathway for o-benzyne$^{\bullet+}$ (the $C_6H_4^{\bullet+}$ isomer shown) dissociating into ($C_4H_2^{\bullet+} + C_2H_2$) and then $C_4H_2^{\bullet+}$ dissociating into ($C_3H^+ + CH^{\bullet}$). The energies of product pairs (P), transitions states (TS), and intermediate minima (I) are given with respect to ground-state benzonitrile$^{\bullet+}$. In addition to the main sequence shown in red, the energies of (o-benzyne$^{\bullet+}$ + CNH, P_2) and ($C_4H_2^{\bullet+} + C_3H_3N$, P_4) are marked. They represent alternative starting points for the subsequent reactions of o-benzyne$^{\bullet+}$ and $C_4H_2^{\bullet+}$. The pathways leading to P_1, P_2, and P_4 from benzonitrile$^{\bullet+}$ have been reported recently (Rap et al. 2023; Kamer et al. 2023), so they are not repeated in this figure.

and argued that these probably resulted from metastable dissociation of o-benzyne$^{\bullet+}$. Hence, the presently observed $C_6H_4^{\bullet+} \rightarrow C_4H_2^{\bullet+} + C_2H_2$ dissociation and our proposed assignment of the precursor to o-benzyne$^{\bullet+}$ are consistent with Liu et al. (2002)'s results and interpretations.

Figure 5 shows a reaction of o-benzyne$^{\bullet+}$ that starts with a ring-opening TS (TS_1) and progresses through further opening of the structure (I_1) prior to dissociation into two symmetric linear products: 1,3−butadiyne$^{\bullet+}$ and acetylene (P_3, the lowest-energy isomers of $C_4H_2^{\bullet+}$ and C_2H_2). This simple reaction involves no CH bond breaking. Kamer et al. (2023)'s calculation of $C_4H_2^{\bullet+}$ production via unimolecular dissociation of benzonitrile$^{\bullet+}$ also yielded 1,3−butadiyne$^{\bullet+}$. The calculated activation energy for that product pair (P_4, 1,3−butadiyne$^{\bullet+}$ and acrylonitrile, C_3H_3N) is 1.73 eV lower than the sequential pathway for 1,3−butadiyne$^{\bullet+}$ production, but this does not necessarily mean that the lower-energy route will dominate when energy deposition is significantly higher than both thresholds. For example, unimolecular CNH loss from benzonitrile$^{\bullet+}$ occurs more frequently than HCN loss in Rap et al. (2023)'s molecular dynamics simulations, despite the latter dissociation having a lower activation energy.

Whereas there is little information in the literature about the dissociation of o-benzyne$^{\bullet+}$, the EI mass spectrum of 1,3−butadiyne (C_4H_2) is available in the NIST database (Wallace 2024). This demonstrates stronger production of C_3H^+ (m/z 37) than $C_3H_2^{\bullet+}$ (m/z 38), which is consistent with band *B* in Table C.3 ($C_4H_2^{\bullet+} \rightarrow CH^{\bullet} + C_3H^+$). Hence, we report the first evidence supporting benzonitrile being a source of methylidyne radicals, and these highly reactive neutrals can participate in diverse interstellar reactions. Figure 5 illustrates the lowest-energy pathway that we identified for this dissociation: a simple cleavage of one of the C=C double bonds.

The second reaction series that we explored theoretically is centered on the $C_6H_2N^+ \rightarrow C_5H^+ + HCN/CNH$ dissociation (corresponding to the intense bands *F* and *P* in Fig. 4). As discussed above, this dissociation is interesting because it represents a new source of interstellar HCN/CNH and because the

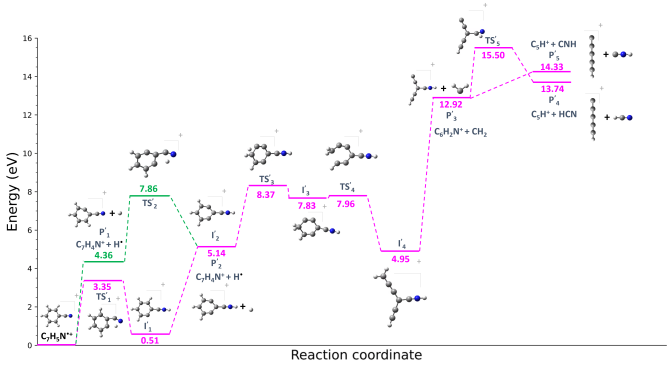

Fig. 6. Calculated reaction pathways starting with $H^{\bullet}$ loss from ground-state benzonitrile$^{\bullet+}$, followed by CH_2 loss and then by CNH loss or HCN loss. Two alternative routes for producing the $C_7H_4N^+$ structure at I'_2 and P'_2 are shown.

present work infers the presence of $C_6H_2N^+$ in the ISM for the first time (Sect. 4.1). Figure 6 shows a reaction pathway that can lead to this dissociation.

We were unable to find a pathway for $C_6H_2N^+$ production via a unimolecular dissociation of benzonitrile$^{\bullet+}$. Figure 2 shows that $C_6H_4CN^+$ (m/z 102) is substantially the most intense fragment ion with m/z ≥ 88, so we consider this to be the most likely precursor for $C_6H_2N^+$ production. Rap et al. (2023) used IR spectroscopy to identify two structures of $C_6H_4CN^+$ (one with an ortho hydrogen removed from benzonitrile$^{\bullet+}$, the other with a meta hydrogen removed). Figure 6 shows ortho–dehydro–benzonitrile$^+$ production (P'_1) instead of meta–dehydro–benzonitrile$^+$ because the former allows a simpler isomerization (via TS'_2) to produce the $C_6H_4CN^+$ structure at I'_2. Rap et al. (2023) did not mention any attempts to detect this symmetric $C_6H_4CN^+$ structure (whereas they explicitly reported seeing no evidence for para hydrogen loss). Alternatively, the same structure can be produced at lower energy cost if isomerization to I'_1 via TS'_1 occurs in benzonitrile prior to P'_2 formation. This isomerization has been reported previously (Rap et al. 2023; Kamer et al. 2023), and occurs at the beginning of four reaction pathways that lead to unimolecular HCN or CNH loss from benzonitrile$^{\bullet+}$.

To our knowledge, no previous publications have addressed the fragmentation of $C_6H_4CN^+$. The present calculations revealed a pathway leading to CH_2 loss via two TSs. TS'_3 involves H transfer to form a CH_2 group at the para position on the ring, and then the ring opens at TS'_4. The ion subsequently relaxes into the 3-arm structure shown at I'_4. CH_2 loss can then proceed directly leaving a 3-arm $C_6H_2N^+$ structure. The production of $C_6H_2N^+$ with CH_2 (P'_3) requires significant energy (around 12.92 eV above the benzonitrile$^{\bullet+}$ ground state), whereas subsequent CNH loss (P'_5) can proceed directly at an additional energy cost of 1.41 eV. Figure 6 also illustrates how hydrogen transfer from N on $C_6H_2N^+$ to its neighboring C (TS'_5) is accompanied by $C_6H_2N^+$ + HCN formation (P'_4). Both of these dissociations result in linear C_5H^+. This ion has not been observed in the ISM to date, but the reaction pathways shown in Fig. 6 followed by collisional neutralization may contribute to the budget of the known interstellar radical l-$C_5H^{\bullet}$ (Cabezas et al. 2022).

5. Astrochemical implications

Comparing fragment ion production in the present MPI experiments with EI experiments (see Appendix B as well as Sect. 4.1) and with DFT calculations (Sect. 4.3) indicates that the reported reaction pathways do not depend critically on the ionization mechanism. Furthermore, all the precursor and product ions identified here in metastable dissociation experiments are also visible in conventional mass spectra showing prompt ion production. This is consistent with the understanding that metastable dissociation experiments reveal dissociations that more typically occur on prompt timescales (when the internal energy of the precursor ion does not happen to be very close to the relevant threshold energy). Hence, the dissociations reported in this paper should be anticipated in any astrophysical environment where gas-phase benzonitrile is exposed to sufficiently energetic photons, electrons, or indeed other types of ionizing radiation (notably fast ions). Cosmic rays and UV photons from nearby stars are important at the edges of molecular clouds (Gredel et al. 1989; Allain et al. 1996; Hollenbach & Tielens 1999). Furthermore, electromagnetic winds generate high energy electrons in the upper atmospheres of planets and moons, including Titan's where benzonitrile's possible presence has attracted particular interest (Khare et al. 1981; Loison et al. 2019).

Efforts to date to model the production and destruction of benzonitrile in cold molecular clouds have predicted abundances that are substantially lower than the observed column densities in the Taurus and Serpens molecular clouds (Burkhardt et al. 2021). Rap et al. (2024) have argued that these underestimations are likely to be due to insufficient physicochemical knowledge of the key molecules involved, notably unknown formation and destruction processes and their accompanying branching ratios and rate coefficients. Each dissociation revealed in this paper is also, when read in reverse, a reaction that can contribute to the synthesis of benzonitrile$^{\bullet+}$ (and thence benzonitrile) wherever the relevant ions and neutrals are present. For example, the present work reveals how the widely observed interstellar molecule acetylene can participate in a reaction pathway leading to benzonitrile$^{\bullet+}$ (see Fig. 5). McGuire and coworkers' models (McGuire et al. 2018; Burkhardt et al. 2021) were based on benzonitrile being dominantly formed via benzene reactions with $CN^{\bullet}$; integrating further reactions into the models may help achieve convergence with the observations.

Two laboratory studies aimed at recreating photolysis- and discharge-driven chemistry in conditions approximating Titan's upper atmosphere have reported benzonitrile production (Khare et al. 1981; Mouzay et al. 2021). Photochemical modeling led Loison et al. (2019) to predict low abundance of benzonitrile in Titan's atmosphere, but the authors noted that the results have large uncertainties due to limited experimental and theoretical data on the diverse pathways leading to the production and destruction of aromatics. The authors also noted that ionic chemistry is expected to play a critical role in the accumulation of benzene in Titan's upper atmosphere. By analogy, this indicates that a thorough characterization of the formation and destruction pathways of benzonitrile$^{\bullet+}$, including the various new reactions identified in the present work, is necessary in order to reliably predict the abundance of benzonitrile in Titan's upper atmosphere as well as its possible roles in the production of other complex molecules.

6. Conclusions

This study provides the first extensive experimental investigation of metastable dissociation following the ionization of benzonitrile. The results confirm three previously reported intense unimolecular dissociations of benzonitrile$^{\bullet+}$ and reveal two new unimolecular dissociations of this astrochemically significant

radical cation. Moreover, we report sequential dissociation pathways from ionized benzonitrile for the first time. The observed dissociations of fragment ions demonstrate new mechanisms by which the irradiation of interstellar benzonitrile produces important reactive species, including CNH, HCN, $CN^{\bullet}$, $CH^{\bullet}$, and $C_3H^{\bullet}$. Furthermore, several of the precursor ions in our observed dissociations have low stabilities, and hence little or no prior information about their fragmentation is available. In particular, we reveal dissociations of $C_6H_2N^+$ and $C_6H_4^{\bullet+}$ that may feature in the sequential dissociative ionization pathways of other interstellar molecules. DFT calculations were carried out to identify reactive pathways that can explain the observed dissociations of these ions. The assignments of specific ions were aided by detailed analyses of peak shapes in a conventional mass spectrum of benzonitrile.

Acknowledgements. The authors are grateful for valuable discussions with Anita Dawes at the OU. The expert technical support provided by T. Webley, K. Dewar, A. Maldonado, and their colleagues at the OU is acknowledged. The OU's logistical and financial support is also acknowledged, including funding DBD's PhD studentship. S.E. acknowledges the British EPSRC's support through a Life Sciences Interface Fellowship (EP/E039618/1), a Career Acceleration Fellowship (EP/J002577/1), and a Research Grant (EP/L002191/1). F.D.S. acknowledges the Portuguese National Funding Agency FCT-MCTES through the research grant number UID/ FIS/00068/2020 (https://doi.org/10.54499/UIDP/00068/2020) (CEFITEC). F.D.S. is also grateful for the funding for project 21GRD02 BIOSPHERE from the European Partnership on Metrology (Funder ID: 10.13039/100019599), co-financed from the European Union's Horizon Europe Research and Innovation Programme and by the Participating States. L.M.C. acknowledges the FAPESP funding agency under process nr. 2020/04822-9. D.B.D. acknowledges the Sir John and Lady Mason Academic Trust for supporting his contributions to experiments in Lisbon.

References

Agúndez, M., Cabezas, C., Marcelino, N., et al. 2022, A&A, 659, L9
Allain, T., Leach, S., & Sedlmayr, E. 1996, A&A, 305, 602
Baldwin, M. A. 1979, Organic Mass Spectr., 14, 601
Barc, B., Ryszka, M., Spurrell, J., et al. 2013, J. Chem. Phys., 139, 244311
Becke, A. 1993, Chem. Phys, 98, 5648
Berné, O., Martin-Drumel, M.-A., Schroetter, I., et al. 2023, Nature, 621, 56
Bocková, J. 2020, Scaling Complexity in the Study of Radiation Damage in Biomolecules (United Kingdom: Open University)
Bockova, J., Rebelo, A., Ryszka, M., et al. 2019, Int. J. Mass Spectr., 442, 95
Burkhardt, A. M., Loomis, R. A., Shingledecker, C. N., et al. 2021, Nat. Astron., 5, 181
Cabezas, C., Agúndez, M., Fuentetaja, R., et al. 2022, A&A, 663, L2
Cernicharo, J., Agúndez, M., Cabezas, C., et al. 2022, A&A, 657, L16
Couturier-Tamburelli, I., Piétri, N., Crépin, C., et al. 2014, J. Chem. Phys., 140, 044329
Daly, F., Douglas-Walker, T., Palotás, J., et al. 2024, J. Chem. Phys., 161, 7
Díaz-Tinoco, M., Dolgounitcheva, O., Zakrzewski, V. G., & Ortiz, J. V. 2016, J. Chem. Phys., 144, 224110
Dopita, M. A., & Sutherland, R. S. 2013, Astrophysics of the Diffuse Universe (Berlin: Springer Science & Business Media)
Frisch, M. J., Trucks, G. W., Schlegel, H. B., et al. 2016, Gaussian~16 Revision C.01 (Wallingford: Gaussian Inc.)
Fukui, K. 1981, Accounts Chem. Res., 14, 363
Gredel, R., Lepp, S., Dalgarno, A., & Herbst, E. 1989, ApJ, 347, 289
Griffiths, I., Mukhtar, E., Harris, F., & Beynon, J. 1981, Int. J. Mass Spectr. Ion Phys., 39, 257
Hendrix, J., Bera, P. P., Lee, T. J., & Head-Gordon, M. 2020, J. Phys. Chem. A, 124, 2001
Hofstein, J., Xu, H., Sears, T., & Johnson, P. 2008, J. Phys. Chem. A, 112, 1195
Hollenbach, D. J., & Tielens, A. 1999, Rev. Mod. Phys., 71, 173
Iglesias-Groth, S. 2023, MNRAS, 523, 2876
Inoue, A., Yoshida, S., & Ebara, N. 1983, Int. J. Mass Spectr. Ion Phys., 52, 209
Jacovella, U., Noble, J. A., Guliani, A., et al. 2022, A&A, 657, A85
Jochims, H.-W., Schwell, M., Baumgärtel, H., & Leach, S. 2005, Chem. Phys., 314, 263
Kamer, J., Schleier, D., Donker, M., et al. 2023, Phys. Chem. Chem. Phys., 25, 29070
Kawaguchi, K., Kasai, Y., Ishikawa, S.-I., et al. 1993, ApJ, 420, L95
Khare, B., Sagan, C., Zumberge, J. E., Sklarew, D. S., & Nagy, B. 1981, Icarus, 48, 290
Langer, W., Velusamy, T., Goldsmith, P., et al. 2017, A&A, 607, A59
Lindon, J., Tranter, G., & Holmes, J. 2000, Encyclopedia of Spectroscopy and Spectrometry, Encyclopedia of Spectroscopy and Spectrometry (Cambridge: Academic Press), 2
Liu, H.-C., Wang, C.-S., Guo, W., Wu, Y.-D., & Yang, S. 2002, J. Am. Chem. Soc., 124, 3794
Loison, J., Dobrijevic, M., & Hickson, K. 2019, Icarus, 329, 55
Mangum, J. G., & Wootten, A. 1990, A&A, 239, 319
Martin, W. B., & O'Malley, R. M. 1984, Int. J. Mass Spectr. Ion Process., 59, 277
McGuire, B. A., Burkhardt, A. M., Kalenskii, S., et al. 2018, Science, 359, 202
McGuire, B. A., Loomis, R. A., Burkhardt, A. M., et al. 2021, Science, 371, 1265
Molenaar-Langeveld, T. A., Fokkens, R. H., & Nibbering, N. M. 1986, Organic Mass Spectr., 21, 15
Mouschovias, T. C., Shu, F., & Woodward, P. 1974, A&A, 33, 73
Mouzay, J., Henry, K., Couturier-Tamburelli, I., et al. 2021, Icarus, 368, 114595
Paron, S., Ortega, M. E., Marinelli, A., Areal, M. B., & Martinez, N. C. 2021, A&A, 653, A77
Pereira-da Silva, J., Rodrigues, R., Ramos, J., et al. 2021, J. Am. Soc. Mass Spectr., 32, 1459
Pety, J., Gratier, P., Guzmán, V., et al. 2012, A&A, 548, A68
Rajasekhar, B., Dharmarpu, V., Das, A. K., et al. 2022, J. Quant. Spectrosc. Radiat. Transf., 283, 108159
Rap, D. B., Simon, A., Steenbakkers, K., et al. 2023, Faraday Discuss., 245, 221
Rap, D. B., Schrauwen, J. G., Redlich, B., & Brünken, S. 2024, Phys. Chem. Chem. Phys., 26, 7296
Ridgway, S. T., Hall, D. N., Kleinmann, S. G., Weinberger, D. A., & Wojslaw, R. S. 1976, Nature, 264, 345
Rosenstock, H. M., Stockbauer, R., & Parr, A. C. 1980, J. Chim. Phys., 77, 745
Ryszka, M., Pandey, R., Rizk, C., et al. 2016, Int. J. Mass Spectr., 396, 48
Schilke, P., Benford, D., Hunter, T., Lis, D., & Phillips, T. 2001, ApJS, 132, 281
Schneider, N., Bonne, L., Bontemps, S., et al. 2023, Nat. Astron., 1, 546
Schug, J. C. 1964, J. Chem. Phys., 40, 1283
Smith, D. 1988, Phil. Trans. R. Soc. London Ser. A Math. Phys. Sci., 324, 257
Tamuliene, J., Romanova, L. G., Vukstich, V. S., Papp, A. V., & Snegursky, A. V. 2015, Euro. Phys. J. D, 69, 1
Van Rossum, G., & Drake, F. L. 2009, Python 3 Reference Manual (Scotts Valley, CA: CreateSpace)
Wallace, W. E. 2024, "Mass Spectra" in NIST Chemistry WebBook, NIST Standard Reference Database Number 69, Eds. P.J. Linstrom and W.G. Mallard, National Institute of Standards and Technology, Gaithersburg MD, 20899, https://doi.org/10.18434/T4D303, (retrieved February 16, 2024)
Ziurys, L. M. 2006, Proc. Natl. Acad. Sci., 103, 12274

Appendix A: Evidence for double ionization products

Three peaks with integer m/z values were visible in the present EI data and in the NIST mass spectrum (Wallace 2024) but were not visible in the present MPI measurements: m/z 43 ($C_2H_5N^+$, C_6N^{2+}, or $C_7H_2^{2+}$), 84 ($C_7^{\bullet+}$), and 85 (C_7H^+; see Fig. 2). This was not due to sensitivity: we were able to achieve higher signal-to-noise ratios in our MPI mass spectra than in our EI mass spectra. Instead, the absence of these peaks in the MPI data can be attributed to high activation energies (notably doubly charged fragment ions, or singly charged fragment ions from doubly charged precursors) that can be accessed in 70 eV collisions but have very low probabilities in the present MPI conditions.

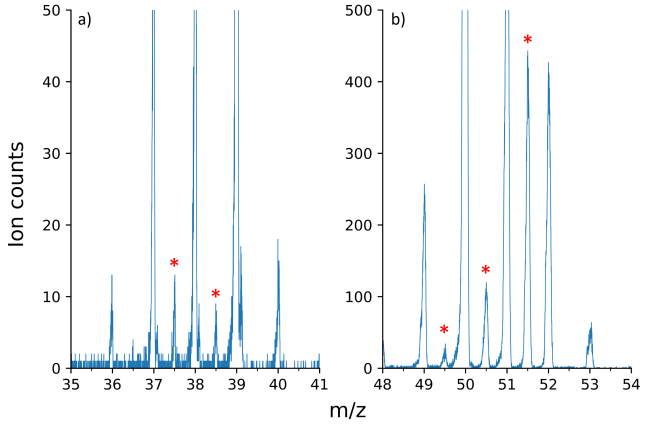

Fig. A.1. Details of the 70 eV EI mass spectrum of benzonitrile. Red stars show doubly charged ions with m/z 37.5 and 38.5 (panel a) and 49.5, 50.5, and 51.5 (benzonitrile$^{\bullet 2+}$; panel b).

Doubly charged benzonitrile has been produced by Griffiths et al. (1981) and our EI experiments confirm that this ion (m/z 51.5; Fig. A.1(b)) is sufficiently stable to survive the journey through the mass spectrometer. To our knowledge, the present EI data provide the first evidence for doubly charged fragment ions from benzonitrile. These have m/z 50.5 ($C_7H_3N^{2+}$), 49.5 (C_7HN^{2+}), 38.5 ($C_6H_5^{2+}$ or $C_5H_3N^{2+}$), and 37.5 (C_5HN^{2+} or $C_6H_3^{2+}$), and are shown in Fig. A.1. We suggest $C_6H_5^{2+}$ and C_5HN^{2+} as the most likely assignments for the m/z 38.5 and 37.5 peaks, based on the assumption that the observed doubly charged ions have the same atomic compositions as the singly charged ions that have been identified with the same masses in the present work and/or previous studies (see our Table C.1; Kamer et al. 2023; Rap et al. 2023). Possible doubly charged ions with even mass numbers (to the nearest integer) cannot be distinguished readily in the present experiment.

Griffiths et al. (1981) reported the following fragment ion pairs from excited doubly charged benzonitrile: (i) $C_6H_4^{\bullet+}$ and $HCN^{\bullet+}$, (ii) $C_6H_3^+$ and H_2CN^+. The first pair mirrors the strongest fragmentation channel of singly charged benzonitrile except that the smaller product is also charged. Indeed, double ionization is the only route that has been reported to date for $HCN^{\bullet+}$ or $CNH^{\bullet+}$ production from benzonitrile. Our Gaussian fitting of the m/z 27 peak in the present MPI experiments demonstrated $C_2H_3^+$ production, and we saw no evidence for $HCN^{\bullet+}/CNH^{\bullet+}$ (see Table C.2). The m/z 27 peak is not clearly enhanced in the EI spectrum compared with the MPI spectrum, so we do not see evidence supporting significant $HCN^{\bullet+}/CNH^{\bullet+}$ production through double ionization.

The m/z values of the second ion pair reported by Griffiths et al. (1981) (m/z 75 and 28) correspond to relatively weak peaks in the present mass spectra and it was not possible to apply Gaussian fitting to confirm the dominant ions in these MPI peaks. Griffiths et al. (1981) assigned the relevant ion pair to $C_6H_3^+$ and H_2CN^+, whereas Kamer et al. (2023) and Rap et al. (2023) reported $HC_5N^{\bullet+}$ and C_2H_4 production from singly ionized benzonitrile. We consider that the most likely assignment for m/z 28 ions from doubly charged ions is $C_2H_4^{\bullet+}$ based on the assumption of analogous dissociation of singly charged benzonitrile. The m/z 75 and 28 signals are stronger compared with their neighboring peaks in the present EI mass spectrum than they are in the present MPI spectrum. This is consistent with these EI peaks containing contributions from the dissociation of doubly charged ions.

Appendix B: Electron ionization metastable dissociation experiments

EI metastable dissociation experiments were carried out at the OU for comparison with the MPI metastable dissociation results (Fig. 4 and Table C.2). A room-temperature effusive beam of benzonitrile vapor was crossed with a pulsed 70 eV electron beam (see Bocková 2020 for details), and the resultant ions were analyzed using a reflectron TOF mass spectrometer with the same geometry as the system shown in Fig. 1. The mapping approach described in Sect. 2 with flight time calculations was applied to identify metastable dissociations in the EI data. Low signal-to-noise ratios compared with the MPI experiments meant that much longer data acquisition times were required, and hence only four reflection voltages were tested. By choosing reflection voltages close to ground, prompt ion signals were also detected and these enabled us to verify the precision of the flight time calculations.

The strongest metastable bands in the EI data are shown in Fig. B.1: m/z 103 → 76 (panel a), m/z 88 → 61 (panel b), and m/z 76 → 50 (panel c). These dissociations also yielded the strongest signals in the MPI metastable dissociation experiments (bands K and S, bands F and P, and bands E and M in Fig. 4). This consistency between the two datasets indicates that these dissociations do not depend on the energy deposition process; only the total energy deposited in benzonitrile$^{\bullet+}$ prior to (unimolecular or sequential) dissociation is important. This is reassuring as we have attached special interest to the m/z 88 → 61 and m/z 76 → 50 dissociations, and they feature in the calculated reaction pathways in Fig. 5 and Fig. 6. The lack of definitive EI evidence for the other dissociations listed in Table C.2 can be attributed to superior signal-to-noise ratios in the MPI data.

Appendix C: Tables

Table C.1. Prompt ions detected from multi-photon ionized benzonitrile (C_6H_5CN): m/z range 61 to 105. Gaussian fits were applied to determine the center m/z values of the peaks that could be assigned to different combinations of atoms.

MPI m/z (nearest integer or center value)	**Present assignments**[@] (with m/z to compare with center value)	**Alternative ion (m/z) that was not identified**[&]	**Previous assignments**	**Relevant ion observations in the ISM**
105	**$^{13}C_2C_5H_5N^{\bullet+}$**	-	[#]	-
104	**$^{13}CC_6H_5N^{\bullet+}$**	-	[#]	-
103	**$C_6H_5CN^{\bullet+}$**	-	[#]	-
102	**$C_7H_4N^+$**	-	$C_7H_4N^+$ (2 structures) (1)	-
101	**$C_7H_3N^{\bullet+}$**	-	[#]	-
100	**$C_7H_2N^+$**	-	[#]	HC_7NH^+ (2)
99	**$C_7HN^{\bullet+}$**	-	[#]	-
98	**C_7N^+**	-	[#]	-
89*	$C_6H_3N^{\bullet+}$ or $C_7H_5^+$	-	-	-
88.015[†]	**$C_6H_2N^+$** (88.019)	$C_7H_4^{\bullet+}$ (88.031)	-	-
87.010[†]	**$C_6HN^{\bullet+}$** (87.011)	$C_7H_3^+$ (87.024)	-	-
86*	C_6N^+ or $C_7H_2^{\bullet+}$	-	-	-
78	$^{13}CC_5H_5^{\bullet+}$ or $^{13}CC_4H_3N^{\bullet+}$	-	-	-
77.040[†]	**$C_6H_5^+$** (77.039) and 25% $^{13}CC_5H_4^{\bullet+}$ (77.035)	$C_5H_3N^{\bullet+}$ (77.027)	$C_6H_5^+$ (1, 3, 4)	-
76*	$C_6H_4^{\bullet+}$ or $C_5H_2N^+$	-	$C_6H_4^{\bullet+}$ (3, 5, 6, 7, 8); 2 structures (1)	-
75*	$C_6H_3^+$ or $C_5HN^{\bullet+}$	-	$HC_5N^{\bullet+}$ (1, 3)	-
74*	$C_6H_2^{\bullet+}$ or C_5N^+	-	-	C_5N^+ (9)
73	**C_6H^+**	-	[#]	-
72	**$C_6^{\bullet+}$**	-	[#]	-
66[%]	**$C_4H_4N^{\bullet+}$**	-	First observed here[$,#]	-
65.026[†]	**$C_4H_3N^{\bullet+}$** (65.027)	$C_5H_5^+$ (65.039)	-	-
64.017[†]	**$C_4H_2N^+$** (64.019)	$C_5H_4^{\bullet+}$ (64.031)	$C_4H_2N^+$ (8)	-
63*	$C_5H_3^+$ or $C_4HN^{\bullet+}$	-	-	-
62*	$C_5H_2^{\bullet+}$ or C_4N^+	-	-	-
61	**C_5H^+**	-	[#]	-

Notes. [(@)]The assignments in bold were identified using Gaussian fits, or they represent the only possible assignment considering the atomic composition of benzonitrile. [(&)]However, a possible weak contribution cannot be ruled out. [(#)]Only one possible assignment. [(*)]Not possible to obtain a good Gaussian fit due to low signal-to-noise ratios or an asymmetric peak shape. [(†)]center value ±0.005. [(%)]The m/z 66 signal is too weak to be discernible in Fig. 2, but we could detect it in an MPI measurement with higher benzonitrile pressure. [($)]These peaks were not visible in the NIST mass spectrum (Wallace 2024) or in Martin & O'Malley (1984)'s mass spectra. References. (1) Rap et al. (2023); (2) Cabezas et al. (2022); (3) Kamer et al. (2023); (4) Molenaar-Langeveld et al. (1986); (5) Schug (1964); (6) Baldwin (1979); (7) Rosenstock et al. (1980); (8) Martin & O'Malley (1984); (9) Cernicharo et al. (2022).

Table C.2. Prompt ions detected from multi-photon ionized benzonitrile: m/z range 1 to 60. Gaussian fits were applied to determine the center m/z values of the peaks that could be assigned to different combinations of atoms.

MPI m/z (nearest integer or center value)	**Present assignments**[@] (with m/z to compare with center value)	**Alternative ion (m/z) that was not identified**[&]	**Previous assignments**	**Relevant ion observations in the ISM**
60	**$C_5^{\bullet+}$**	-	[#]	-
53.042[†]	**$C_4H_5^+$** (53.039)	$C_3H_3N^{\bullet+}$ (53.027)	-	-
52.035[†]	**$C_4H_4^{\bullet+}$** (52.031)	$C_3H_2N^+$ (52.019)	$C_4H_4^{\bullet+}$ (1, 2)	$C_3NH_2^+$ (3)
51.022[†]	**$C_4H_3^+$** (51.024) and 5% $^{13}CC_3H_2^{\bullet+}$ (51.019)	$C_3HN^{\bullet+}$ (51.011)	$C_4H_3^+$ (1, 2)	-
50.017[†]	**$C_4H_2^{\bullet+}$** (50.016)	C_3N^+ (50.003)	$C_4H_2^{\bullet+}$ (1, 2)	-
49	**C_4H^+**	-	[#]	-
48	**$C_4^{\bullet+}$**	-	[#]	-
40.031[†]	**$C_3H_4^{\bullet+}$** (40.031)	$C_2H_2N^+$ (40.019)	-	-
39.026[†]	**$C_3H_3^+$** (39.024)	$C_2HN^{\bullet+}$ (39.011)	$C_3H_3^+$ (2)	-
38.012[†]	**$C_3H_2^{\bullet+}$** (38.016)	C_2N^+ (38.003)	-	-
37	**C_3H^+**	-	[#]	C_3H^+ (4)
36	**$C_3^{\bullet+}$**	-	[#]	-
28*	$C_2H_4^{\bullet+}$ or CH_2N^+	-	First observed here[$]	H_2CN^+ (5), $HCNH^+$ (6)
27.020[†]	**$C_2H_3^+$** (27.024)	$HCN^{\bullet+}$ (27.011)	-	-
26.013[†]	**$C_2H_2^{\bullet+}$** (26.016)	$CN^{\bullet\bullet+}$ (26.003)	$C_2H_2^{\bullet+}$ (2)	$CN^{\bullet\bullet+}$ (7)
25	**C_2H^+**	-	[#]	-
24	**$C_2^{\bullet+}$**	-	[#]	-
15.024[†]	**CH_3^+** (15.024)	$HN^{\bullet+}$ (15.011)	-	CH_3^+ (8), /-CH_3^+ (9)
14.016[†]	**$CH_2^{\bullet+}$** (14.016)	N^+ (14.003)	-	N^+ (10)
13	**CH^+**	-	[#]	CH^+ (5)
12	**$C^{\bullet+}$**	-	[#]	$C^{\bullet+}$ (11)
1	**H^+**	-	First observed here[$],[#]	H^+ (12)

Notes. [(@)]The assignments in bold were identified using Gaussian fits, or they represent the only possible assignment considering the atomic composition of benzonitrile. [(&)]However, a possible weak contribution cannot be ruled out. [(#)]Only one possible assignment. [(†)]center value ±0.005. [(*)]Not possible to obtain a good Gaussian fit due to low signal-to-noise ratios or an asymmetric peak shape. [($)]These peaks were not visible in the NIST mass spectrum (Wallace 2024) or in Martin & O'Malley (1984)'s mass spectra. References. (1) Kamer et al. (2023); (2) Martin & O'Malley (1984); (3) Agúndez et al. (2022); (4) Cernicharo et al. (2022); (5) Smith (1988); (6) Kawaguchi et al. (1993); (7) Dopita & Sutherland (2013); (8) Berné et al. (2023); (9) Pety et al. (2012); (10) Langer et al. (2017); (11) Schneider et al. (2023); (12) Mouschovias et al. (1974).

Table C.3. Metastable dissociations observed in our MPI experiments on benzonitrile.

Precursor ion and product ion (m/z)	**Neutral product** (amu)	**Assigned dissociation**	**Fig. 4 bands**	**Comments and any previous evidence**
49 ⟶ 37	12	$C_4H^+ \longrightarrow C_3H^+ + C$	A	First evidence for C from benzonitrile.
50 ⟶ 37	13	$C_4H_2^{\bullet+} \longrightarrow C_3H^+ + CH^\bullet$	B	-First evidence for $CH^\bullet$ from benzonitrile. -See the calculated sequence in Fig. 5.
64 ⟶ 37	27	$C_5H_4^{\bullet+} \longrightarrow C_3H^+ + C_2H_3^\bullet$ or $C_4H_2N^+ \longrightarrow C_3H^+ + HCN/CNH$	C	
73 ⟶ 36	37	$C_6H^+ \longrightarrow C_3^{\bullet+} + C_3H^\bullet$	D	First evidence for $C_3H^\bullet$ from benzonitrile.
75 ⟶ 49	26	$C_5HN^{\bullet+} \longrightarrow C_4H^+ + CN^\bullet$	L	New route for $CN^\bullet$ production.
76 ⟶ 50	26	$C_6H_4^{\bullet+} \longrightarrow C_4H_2^{\bullet+} + C_2H_2$	E & M	-First evidence for C_2H_2 from benzonitrile. -See the calculated sequence in Fig. 5.
77 ⟶ 51	26	$^{13}CC_5H_4^+ \longrightarrow {}^{13}CC_3H_2^+ + C_2H_2$	N	#
87 * ⟶ 60 or 86 ⟶ 60	27 or 26	$C_6HN^{\bullet+} \longrightarrow C_5^{\bullet+} + HCN/CNH$ or $C_6N^+ \longrightarrow C_5^{\bullet+} + CN^\bullet$ or $C_7H_2^{\bullet+} \longrightarrow C_5^{\bullet+} + C_2H_2$	O	
88 ⟶ 61	27	$C_6H_2N^+ \longrightarrow C_5H^+ + HCN/CNH$	F & P	-New route for HCN/CNH production. -See the calculated sequence in Fig. 6.
89 ⟶ 62	27	$^{13}CC_5H_2N^+ \longrightarrow {}^{13}CC_4H^+ + HCN/CNH$	Q	#
100 ⟶ 74	26	$C_7H_2N^+ \longrightarrow C_6H_2^{\bullet+} + CN^\bullet$ or $C_7H_2N^+ \longrightarrow C_5N^+ + C_2H_2$	J & R	
103 ⟶ 37 * or 103 ⟶ 38	66 or 65	$C_6H_5CN^{\bullet+} \longrightarrow C_3H^+ + C_4H_4N^\bullet$ or $C_6H_5CN^{\bullet+} \longrightarrow C_3H_2^{\bullet+} + C_4H_3N$ or $C_6H_5CN\cdot^+ \longrightarrow C_2N^+ + C_5H_5^\bullet$	G	The possible neutral products ($C_4H_4N^\bullet, C_4H_3N, C_5H_5^\bullet$) have not been observed before from benzonitrile or in the ISM.
103 ⟶ 50	53	$C_6H_5CN^{\bullet+} \longrightarrow C_4H_2^{\bullet+} + C_3H_3N$	H	Photoionization (1)
103 ⟶ 62	41	$C_6H_5CN^{\bullet+} \longrightarrow C_5H_2^{\bullet+} + C_2H_3N$ or $C_6H_5CN^{\bullet+} \longrightarrow C_4N^+ + C_3H_5^\bullet$	I	The possible neutral products ($C_2H_3N, C_3H_5^\bullet$) have not been observed before from benzonitrile.
103 ⟶ 76	27	$C_6H_5CN^{\bullet+} \longrightarrow C_6H_4^{\bullet+} + HCN/CNH$	K & S	-Metastable dissociation (2, 3), photoionization (1). -See the calculated sequence in Fig. 5.
103 ⟶ 77£	26	$C_6H_5CN^{\bullet+} \longrightarrow C_6H_5^+ + CN^\bullet$	T	Photoionization (1)
104 ⟶ 77	27	$^{13}CC_6H_5N^{\bullet+} \longrightarrow {}^{13}CC_5H_4^{\bullet+} + HCN/CNH$		

Notes. (*)Figure 4 includes the simulated flight times for the m/z 87 → 60 and m/z 103 → 37 dissociations, but the m/z 86 → 60 and m/z 103 → 38 dissociations show similarly good agreement with the experimental bands O and G. (#)Bands N and Q are assigned to isotopes based on their intensities compared with bands M and P, respectively. (£)The ratio of band T over band S (17%) is much bigger than the predicted ratio based on the isotope distribution (8%). Therefore, there must be a contribution to this band from another type of metastable dissociation. The only candidate whose simulated flight times overlap with this band is m/z 103 → 77. References. (1) Kamer et al. (2023); (2) Schug (1964); (3) Baldwin (1979).

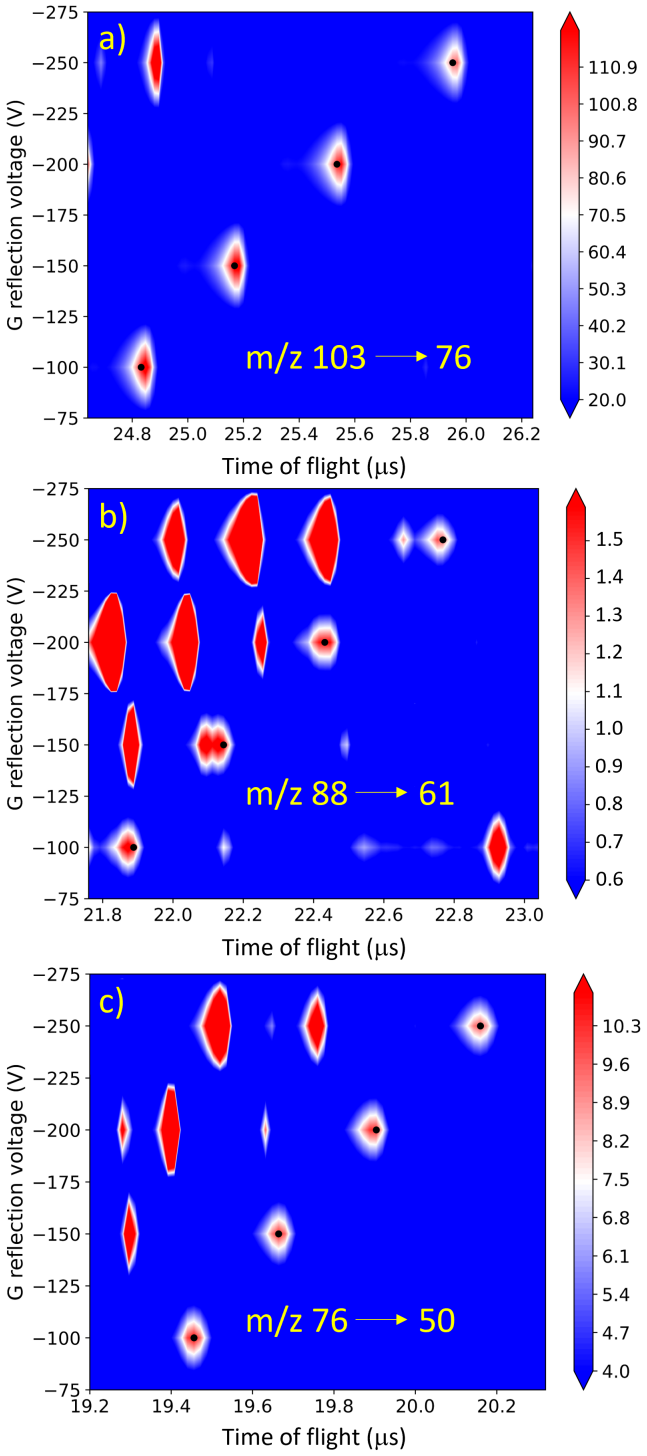

Fig. B.1. 70 eV EI signals from benzonitrile mapped against flight time and the reflection voltage applied to Grid G in the mass spectrometer (see Fig. 1(b)). The signals (ion counts per 16 ns time bin) are indicated by red and white features. The simulated flight times for metastable dissociations that agree best with selected experimental bands (m/z 103 → 76, m/z 88 → 61, and m/z 76 → 50) are indicated by black dots. Unlike Fig. 4, signals due to prompt dissociations are visible in these maps, as are signals due to metastable dissociations.